AD-A187 004 CORONAL HEATING BY MEANS OF HELICAL MAGNETOHYDRODYNAMIC TURBULENCE(U) NAVAL RESEARCH LAB WASHINGTON DC R B DAHLBURG ET AL. 17 DEC 87 NRL-MR-6073 1/1

UNCLASSIFIED F/G 20/9 NL

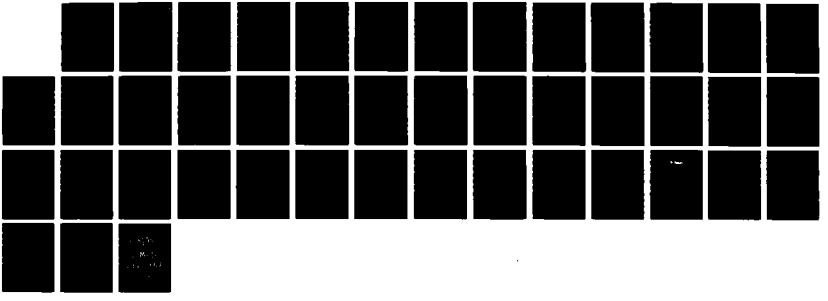

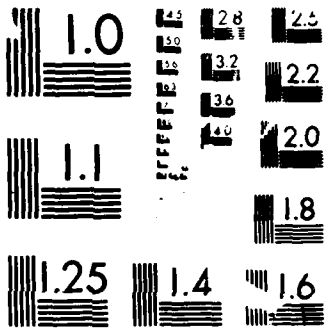

Naval Research Laboratory

Washington, DC 20375-5000

2

NRL Memorandum Report 6073

Coronal Heating by Means of Helical Magnetohydrodynamic Turbulence

R. B. DAHLBURG AND J. P. DAHLBURG

Laboratory for Computational Physics

J. T. MARISKA

E. O. Hulburt Center for Space Research

December 17, 1987

Approved for public release; distribution unlimited

SECURITY CLASSIFICATION OF THIS PAGE

REPORT DOCUMENTATION PAGE

1a. REPORT SECURITY CLASSIFICATION UNCLASSIFIED	1b. RESTRICTIVE MARKINGS
2a. SECURITY CLASSIFICATION AUTHORITY	3. DISTRIBUTION / AVAILABILITY OF REPORT Approved for public release; distribution unlimited.
2b. DECLASSIFICATION / DOWNGRADING SCHEDULE	
4. PERFORMING ORGANIZATION REPORT NUMBER(S) NRL Memorandum Report 6073	5. MONITORING ORGANIZATION REPORT NUMBER(S)
6a. NAME OF PERFORMING ORGANIZATION Naval Research Laboratory 6b. OFFICE SYMBOL (If applicable) Code 4440	7a. NAME OF MONITORING ORGANIZATION NASA
6c. ADDRESS (City, State, and ZIP Code) Washington, DC 20735-5000	7b. ADDRESS (City, State, and ZIP Code) Washington, DC 20546
8a. NAME OF FUNDING / SPONSORING ORGANIZATION NASA 8b. OFFICE SYMBOL (If applicable)	9. PROCUREMENT INSTRUMENT IDENTIFICATION NUMBER
8c. ADDRESS (City, State, and ZIP Code) Washington, DC 20546	10. SOURCE OF FUNDING NUMBERS PROGRAM ELEMENT NO. W-15633 / PROJECT NO W-15633 / TASK NO NASA / WORK UNIT ACCESSION NO 44-0985

11. TITLE (Include Security Classification)
Coronal Heating by Means of Helical Magnetohydrodynamic Turbulence

12. PERSONAL AUTHOR(S)
Dahlburg, R. B., Dahlburg, J. P., and Mariska, J. T.

13a. TYPE OF REPORT	13b. TIME COVERED	14. DATE OF REPORT (Year, Month, Day)	15. PAGE COUNT
Interim	FROM 10/1/86 TO present	1987 December 17	43

16. SUPPLEMENTARY NOTATION

17. COSATI CODES			18. SUBJECT TERMS (Continue on reverse if necessary and identify by block number)
FIELD	GROUP	SUB-GROUP	Coronal Heating, Helical Magnetohydrodynamic Turbulence, Direct Numerical Simulation

19. ABSTRACT (Continue on reverse if necessary and identify by block number)

We investigate by means of numerical simulations the relaxation of an unconfined, helically turbulent, fully three-dimensional magnetofluid, with conditions similar to those which are thought to result in the heating of the solar corona. In these simulations, the system evolves through a succession of force-free states. After a relatively quiescent period of Ohmic decay, a phase of accelerated magnetic energy dissipation occurs. Some magnetic energy is transformed into kinetic energy, and the magnitude of enstrophy created is a nontrival fraction of the mean square electric current. Concentrated vorticity structures are seen to play almost as important a role as electric current sheets in the heating process. Coincident with this accelerated dissipation process, a reorganization of the magnetic field occurs, with transfer of magnetic energy to both shorter and longer wavelength modes than are initially present. The ratio of the magnetic field to the electric current density, α, does not in general tend to assume a constant value in the force-free regions during the evolution of the magnetofluid.

20. DISTRIBUTION / AVAILABILITY OF ABSTRACT ☒ UNCLASSIFIED/UNLIMITED ☐ SAME AS RPT ☐ DTIC USERS	21. ABSTRACT SECURITY CLASSIFICATION UNCLASSIFIED
22a. NAME OF RESPONSIBLE INDIVIDUAL Russell B. Dahlburg	22b. TELEPHONE (Include Area Code) 202-767-0608 / 22c. OFFICE SYMBOL 4440

DD FORM 1473, 84 MAR 83 APR edition may be used until exhausted
All other editions are obsolete

SECURITY CLASSIFICATION OF THIS PAGE

*U.S. Government Printing Office: 1988—607-047

CONTENTS

Coronal Heating by Means of Helical Magnetohydrodynamic Turbulence

1. Introduction

This paper reports the results of numerical simulation of the viscoresistive decay of helically turbulent magnetofluids. This decay process has recently come to be of interest because of the possibility that it might contribute to the heating of the solar corona. It is by now generally accepted that the corona is heated by the dissipation of magnetic energy (see, *e. g.*, Chapter 6 of Priest 1982 and references therein). The coronal magnetic field is believed to be continually perturbed as the footpoints of the coronal flux tubes are convected about by the turbulent motions of the nearly ideal, high β, photospheric plasma. Both random displacements and helical, twisting motions (perhaps by Coriolis forces due to solar rotation) are possible. These magnetic field disturbances propagate into the corona, driving the plasma there into an excited, nonequilibrium state. As the plasma settles into a new, quiescent state, the magnetic energy is released directly as heat energy by Ohmic dissipation and indirectly by viscous dissipation of the induced fluid motions. The characteristic structure associated with this dissipation is the familiar electric current sheet located at a region where the magnetic field changes sign (*e.g.*, Syrovatskii 1978, Matthaeus and Montgomery 1981, R. Dahlburg *et al.* 1986*a*, Spicer *et al.* 1986).

Only a small portion of the magnetic energy in the corona ends up being transformed into heat. The overwhelming portion exists in fairly long lived structures, most of which is in the form of coronal loops. The observed stability of these structures, as well as the low β character of the corona, suggests that they are force-free configurations, *i.e.*, configurations in which the magnetic field, $\mathbf{B}$, satisfies the equation $\nabla \times \mathbf{B} = \alpha \mathbf{B}$, with $\alpha = \alpha(\mathbf{x}, t)$. Hence the disturbances in the coronal magnetic field induced by the motions of the footpoints can be thought of as perturbations on

Manuscript approved June 18, 1987.

a force-free state. The relative stability of the coronal magnetic field suggests that the perturbed system then relaxes to a new, force-free state. Noting this, Heyvaerts and Priest (1984) adapted to the solar corona a theory developed by Taylor (1974) for relaxation to force-free, minimum energy states in the reversed field pinch, a magnetic confinement fusion device. The details of Taylor's theory are provided in their paper (see also the recent review by Taylor 1986). Assuming that the coronal magnetic field is helical and approximately force-free, Heyvaerts and Priest used Taylor's method to determine to what state the perturbed coronal magnetic field would relax. Using the assumption that the kinetic energy and internal energy are negligible with respect to the magnetic energy, they minimized the total energy in the magnetofluid subject to the constraint that the magnetic helicity remain constant, and obtained constant α, force-free minimum energy states. The magnetic energy dissipated as heat could then be determined by comparing the initial magnetic field with the minimum energy state magnetic field. The heating is produced by the dissipation of magnetic energy at electric current sheets which are formed locally in the corona. These ideas were extended and developed by Browning *et al.* (1986) and Browning and Priest (1986).

The theories of Taylor (1974) and Heyvaerts and Priest (1984) are based on the stability of the final magnetic field configuration, with no consideration of the evolution of the magnetofluid toward a force-free state. This dynamic relaxation process is now thought to occur as a consequence of the self-organization of the helically turbulent magnetofluid. Because our results are interpreted in terms of this relaxation theory, we review certain relevant details in Sect. 2 (see also the recent review by Hasegawa 1985 and references therein). We note here certain artificial constraints which the Taylor-Heyvaerts theory places on the magnetofluid. This

Taylor-Heyvaerts analysis assumes that the kinetic energy will remain very small with respect to the magnetic energy at all times of the magnetofluid evolution, and that α will tend toward constant values. However, Low (1982) has suggested that non-constant α, force-free magnetic fields are more common. This follows as a consequence of the fact that the constant α magnetic field obeys the linear vector Helmholtz equation $\nabla^2\mathbf{B} + \alpha^2\mathbf{B} = 0$, which has a smaller set of solutions that is contained in the set of solutions of the more general force-free field equation, $\nabla \times \mathbf{B} = \alpha\mathbf{B}$, where α can vary. Furthermore, J. Dahlburg *et al.* (1986*b*, 1987) report the observation of significant kinetic energy formation, followed by the attainment of a force-free, lower energy state characterized by nonconstant α, in numerical simulations of the reversed-field pinch fusion device. Hence, it is important to follow the nonlinear evolution of a fully three-dimensional, unbounded, corona-like magnetofluid to determine: (1) if such magnetofluids tend to evolve through a succession of force-free states when perturbed away from a force-free state; (2) if the approach to such states results in enhanced heat production; (3) if the velocity field plays a significant role in the dissipative process; and (4) if any lower energy states which occur are also constant α states. We also want to observe the structural consequences of the nonlinear evolution of the magnetofluid, and to determine what structures contribute to the heating.

We here report results from fully three-dimensional, single-fluid MHD simulations in periodic geometry which help to answer these questions. We consider an initial value problem with a helical force-free magnetic field perturbed by random noise in the velocity and magnetic fields. Study of the initial value problem is similar in spirit to the "mixing time" approach of Heyvaerts and Priest (1984). The system is assumed to be periodic, so no effects due to confinement are possible.

We follow the evolution of this system and determine the extent and character of the accelerated heating which occurs due to turbulent transfer of excitations. In Sect. 3 we give the initial conditions and boundary conditions. The results of the numerical simulations are described in Sect. 4. In Sect. 5 we discuss the results. Our numerical method is described in the appendix.

2. Review of turbulent self-organization

The nonlinear partial differential equations that govern the behavior of a three-dimensional, viscoresistive, incompressible magnetofluid, written in a dimensionless, rotation form, are:

$$\frac{\partial \mathbf{v}}{\partial t} = \mathbf{v} \times \omega - \nabla \Pi + \mathbf{J} \times \mathbf{B} + \frac{1}{M} \nabla^2 \mathbf{v} = \mathbf{H}\,, \tag{1a}$$

$$\nabla \cdot \mathbf{v} = 0\,, \tag{1b}$$

$$\frac{\partial \mathbf{A}}{\partial t} = \mathbf{v} \times \mathbf{B} + \nabla \Phi + \frac{1}{S} \nabla^2 \mathbf{A} = \mathbf{G}\,, \tag{1c}$$

$$\nabla \cdot \mathbf{A} = 0\,, \tag{1d}$$

where $\mathbf{v}(\mathbf{x},t) \equiv$ flow velocity, $\omega(\mathbf{x},t) = \nabla \times \mathbf{v} \equiv$ vorticity, $\mathbf{A}(\mathbf{x},t) \equiv$ magnetic vector potential, $\mathbf{B}(\mathbf{x},t) = \nabla \times \mathbf{A} \equiv$ magnetic field, $\mathbf{J}(\mathbf{x},t) = \nabla \times \mathbf{B} \equiv$ electric current density, $\Pi(\mathbf{x},t) \equiv$ pressure head, $\Phi(\mathbf{x},t) \equiv$ a magnetic scalar potential, $S \equiv$ Lundquist number, and $M \equiv$ viscous Lundquist number. The Coulomb gauge is assumed. In this representation, $\mathbf{B}$ is measured in terms of a characteristic field strength, *e.g.*, $B_0 = \left(V^{-1} <\mid \mathbf{B} \mid^2>\right)^{\frac{1}{2}}$, where the brackets $<>$ indicate an integral over the system and V denotes the volume of integration. The velocities are measured in units of the Alfvén speed, $C_A = \frac{B_0}{(4\pi\rho)^{\frac{1}{2}}}$ where the mass density, ρ, is assumed to be constant and uniform. For a characteristic distance, L_0, the time is measured in units of the Alfvén transit time, $\frac{L_0}{C_A}$. The Lundquist number

$S = \frac{c_A L_0}{\eta}$, where η is the magnetic diffusivity. The viscous Lundquist number $M = \frac{c_A L_0}{\nu}$, where ν is the kinematic viscosity. The Lundquist numbers express the ratio between the convective terms and the dissipative terms (for a fuller discussion of the importance of the Lundquist numbers, see R. Dahlburg *et al.* (1983)).

For the ideal magnetofluid, $S \rightarrow \infty$ and $M \rightarrow \infty$. In this limit there is no dissipation. There are known to be three conserved, global quantities for the three-dimensional, ideal magnetofluid (*e.g.*, Frisch *et al.* 1975). These are the total energy:

$$E_T = \frac{1}{2} \int_0^{2\pi} \int_0^{2\pi} \int_0^{2\pi} \left(| \mathbf{v} |^2 + | \mathbf{B} |^2 \right) dx\, dy\, dz, \tag{2a}$$

the magnetic helicity:

$$H_M = \int_0^{2\pi} \int_0^{2\pi} \int_0^{2\pi} \mathbf{A} \cdot \mathbf{B}\, dx\, dy\, dz, \tag{2b}$$

and the cross helicity (sometimes called the cross energy):

$$H_C = \int_0^{2\pi} \int_0^{2\pi} \int_0^{2\pi} \mathbf{v} \cdot \mathbf{B}\, dx\, dy\, dz, \tag{2c}$$

where periodic boundary conditions are assumed. These quantities also remain invariant if perfectly conducting and/or free-slip boundary conditions are assumed in any or all of the three directions.

These ideal constants of motion are of great importance in the statistical theory of MHD turbulence because their Fourier transforms define hypersurfaces in the complex Fourier space of coefficients of the magnetic and velocity fields. The volume averaged, Fourier representations of the ideal invariants are:

$$E_T = \frac{1}{2}\sum_{\mathbf{k}}\Big[\mid \mathbf{v}(\mathbf{k},t)\mid^2 + \mid \mathbf{B}(\mathbf{k},t)\mid^2\Big], \tag{3a}$$

$$H_M = \sum_{\mathbf{k}}\Big[\mathbf{A}^*(\mathbf{k},t)\cdot\mathbf{B}(\mathbf{k},t)\Big], \tag{3b}$$

and,

$$H_C = \sum_{\mathbf{k}}\Big[\mathbf{v}^*(\mathbf{k},t)\cdot\mathbf{B}(\mathbf{k},t)\Big], \tag{3c}$$

where the superscript "*" denotes the complex conjugate and k is the Fourier wavenumber.

The behavior of the turbulent ideal magnetofluid will depend strongly on the relative magnitudes of these invariants. For example, consider the case in which the magnetic energy is much greater than the kinetic energy, the situation in the solar corona. This implies that the cross helicity will be negligible, since the magnitude of the velocity field will be small. Furthermore, the total energy will consist almost exclusively of magnetic energy, since in this case $\mid \mathbf{B}\mid^2 >> \mid \mathbf{v}\mid^2$.

In the presence of finite dissipation, the total energy, E_T, and the magnetic helicity, H_M, will decay according to the following equations (*e.g.*, Matthaeus and Montgomery 1980):

$$\frac{dE_T}{dt} = -\frac{1}{S}\int_0^{2\pi}\int_0^{2\pi}\int_0^{2\pi} \mid \mathbf{J}\mid^2 \, dx\,dy\,dz - \frac{1}{M}\int_0^{2\pi}\int_0^{2\pi}\int_0^{2\pi} \mid \omega\mid^2 \, dx\,dy\,dz\,, \tag{4a}$$

and,

$$\frac{dH_M}{dt} = -\frac{1}{S}\int_0^{2\pi}\int_0^{2\pi}\int_0^{2\pi} \mathbf{J}\cdot\mathbf{B}\,dx\,dy\,dz. \tag{4b}$$

The first integral on the right hand side of equation $4a$ is called the mean square electric current, and it determines the rate at which the magnetic energy is dissipated. The second integral on the right hand side of equation $3a$ is called the enstrophy, and it determines the rate at which the kinetic energy is dissipated. For the $|\mathbf{B}|^2 >> |\mathbf{v}|^2$ case, the enstrophy is much smaller than the mean square electric current. Hence, for a unit magnetic Prandtl number the viscous dissipation of energy should be negligible. The Fourier space representation of these decay laws is:

$$\frac{dE_T}{dt} = -\frac{1}{S}\sum_{\mathbf{k}} |\,\mathbf{J}(\mathbf{k},t)\,|^2 - \frac{1}{M}\sum_{\mathbf{k}} |\,\omega(\mathbf{k},t)\,|^2, \tag{5a}$$

and,

$$\frac{dH_M}{dt} = -\frac{1}{S}\sum_{\mathbf{k}}\left[\mathbf{J}^*(\mathbf{k},t)\cdot\mathbf{B}(\mathbf{k},t)\right]. \tag{5b}$$

Now consider, for example, a force-free case in which the magnetic vector potential, the magnetic field, and the electric current density are all directly proportional to each other initially (we will consider such a case in this paper). In this case the ratio E_T/H_M will remain constant as the magnetic field decays by means of Ohmic diffusion. When perturbed, however, the system will execute a more complex evolution due to the activation of the nonlinear terms in the governing equations. As the system evolves nonlinearly the magnetic field excitations will tend to spread

out in wavenumber space due to interactions among resonant triads of wavevectors. The electric current density, $\mathbf{J}(\mathbf{k})$ will populate the shorter wavelengths at a rate faster than the magnetic field, $\mathbf{B}(\mathbf{k})$, since $\mathbf{J}(\mathbf{k}) = i\mathbf{k} \times \mathbf{B}(\mathbf{k})$. For $k > 1$, $\mathbf{J}^*(\mathbf{k}) \cdot \mathbf{J}(\mathbf{k})$ will tend to be larger in magnitude than $\mathbf{J}^*(\mathbf{k}) \cdot \mathbf{B}(\mathbf{k})$. Furthermore, $\mathbf{J} \cdot \mathbf{J}$ is positive definite, while $\mathbf{J} \cdot \mathbf{B}$ can be negative. All this implies that a selective decay of the magnetic energy will take place with respect to the magnetic helicity once the turbulent transport of excitations becomes significant (Montgomery *et al.* 1978). Consequently the ratio E_T/H_M should decrease as a function of time when the system becomes turbulent.

Finally, the nonlinear mode coupling is such that the magnetic helicity, which suffers less dissipation than the total energy, is preferentially transferred to the longest wavelengths of the system (Frisch *et al.* 1975, Pouquet *et al.* 1976, Montgomery *et al.* 1978). This transfer of magnetic helicity to smaller wavenumbers finds morphological expression in the tendency of the magnetic field to assume long-wavelength structures. The transfer of total energy to larger wavenumbers finds morphological expression in the formation of electric current sheets and concentrated vorticity structures. These current sheets and concentrated vorticity structures are the primary sites at which turbulent heating occurs.

The final state the relaxing magnetofluid is thought to assume is a minimum-energy, force-free state, commonly referred to as a "Taylor state." These final states have been discussed by Taylor (1974) and Heyvaerts and Priest (1984), who considered stability properties alone. By minimizing the magnetic energy subject to the constraint of constant magnetic helicity, Taylor showed that the minimum energy state to be obtained would be a constant α state, where $\nabla \times \mathbf{B} = \alpha \mathbf{B}$. Although the evolution toward a force-free state has been found to occur in computer simulations

by J. Dahlburg *et al.* (1987) in reversed-field pinch-like geometry, questions remain with respect to the low velocity and constant α assumptions, as well as the possibility of evolution toward a force-free state in situations in which rigid, perfectly conducting, impenetrable walls are not present, *e.g.*, in the solar corona.

3. Formulation of the problem

For the initial background, force-free magnetic field we use the following prescription of the magnetic vector potential:

$$A_x(\mathbf{x}, t = 0) = C_1 \sin x \cos y \,, \tag{6a}$$

$$A_y(\mathbf{x}, t = 0) = -C_1 \cos x \sin y \,, \tag{6b}$$

$$A_z(\mathbf{x}, t = 0) = C_2 \sin x \sin y \,, \tag{6c}$$

where $C_1 = 0.5$ and $C_2 = C_1^{0.5}$. No current sheets are present initially in this magnetic field configuration. Note that initially $\nabla \times \mathbf{B} = \alpha \mathbf{B}$, with $\alpha = 2^{0.5}$ throughout the system (in fact, $\nabla^2 \mathbf{B} + \alpha^2 \mathbf{B} = 0$, and this is a linear, constant α, force-free magnetic field). The initial, unperturbed, volume averaged magnetic energy equals 1. The initial, unperturbed, volume averaged magnetic helicity equals $\frac{1}{\alpha} = 2^{-0.5}$.

This configuration ($6a - 6c$) will simply decay Ohmically if unperturbed, since fluid motion will be excited because it is force-free. We perturb this configuration with broad-band noise in both the velocity and magnetic field to ensure a nontrivial evolution. This allows the system to traverse as wide a range of the available phase space as possible. The fastest growing disturbances, whatever they might be, emerge naturally from the noise as time advances. These initial conditions are similar to those used by Horiuchi and Sato (1985, 1986).

Periodic boundary conditions are enforced in all three spatial directions. It seems wisest to use these boundary conditions so that the turbulent magnetofluid can be simulated with the greatest accuracy, *i.e.*, without the need to use special measures to enforce more specific boundary conditions (*cf.* Meneguzzi *et al.* 1981, Pouquet *et al.* 1986). The restriction to periodic boundary conditions, coupled with our use of a Fourier pseudospectral numerical algorithm, allow us to obtain high resolution of the turbulent evolution of the magnetofluid. The fully three-dimensional, Fourier pseudospectral, numerical simulation code used to advance the governing equations, $1a - 1d$, is described in the appendix.

4. Results of numerical simulations

In this section we describe the results from a typical simulation, which is representative of about ten simulations that we have performed. The spatial grid uses 32^3 Fourier modes, with a time step of 1/500. At this size the code requires about 1.5 seconds per time step on the CRAY-2, and approximately 1.2 million words of memory. The Lundquist numbers are set to 400 for this run. On the basis of the Kolmogorov dissipation wavenumber, this is close to the limit at which we can accurately compute the turbulent evolution of the magnetofluid. In fact, accurate numerical simulation of two-dimensional turbulent magnetofluids has been limited to Lundquist numbers of about 1000 on the present generation of computers (*e.g.*, Forbes and Priest 1983) and to Lundquist numbers of less than 500 for the three-dimensional case (J. Dahlburg *et al.*, 1987). These Lundquist numbers are well above the known linear stability boundaries for magnetic reconnection to occur (R. Dahlburg *et al.* 1983, Bondeson and Sobel 1984).

We first describe the evolution of the magnetofluid with the assistance of the global diagnostics, and then discuss the structural evolution. Figure 1 shows E_B, E_V, H_M, and E_T/H_M as functions of time. All global quantities shown are volume averaged. The magnetic energy in the configuration described by equations 6*a* – 6*c* is equal to 1. The initial kinetic energy and the perturbed magnetic energy each are equal to 0.25×10^{-3}, with the band of excitation given by $9 \leq \mid \mathbf{k} \mid^2 \leq 1000$. Hence the energy in the perturbation is 0.05 % of the background magnetic configuration given by equations $6a - 6c$. The magnetic energy, E_B, first decays Ohmically for about twenty Alfvén transit times. At this time, turbulent activity begins and accelerated dissipation of E_B occurs. The lost magnetic energy is both dissipated

and transformed into kinetic energy. Following this, some dynamo activity is observed as the magnetic energy resumes decaying at a slower rate. The kinetic energy, E_V, remains relatively small until the accelerated decay of the magnetic energy occurs. At this time a rapid buildup of kinetic energy occurs, indicative of organized fluid motions. After several bursts of activity, the kinetic energy dies off. The magnetic helicity, H_M, decays relatively slowly throughout the run, with relatively little variation in response to the magnetofluid activity. Of perhaps more importance is the ratio of the total energy to the magnetic helicity, E_T/H_M. In figure 1 we normalize this ratio to its initial value of 1.414. This ratio remains approximately constant until the onset of turbulent activity, indicating that the decay of the total energy and the magnetic helicity at early times is being determined by the linear, dissipative terms. The decline in the value of this ratio indicates the onset of turbulent activity, in which the total energy is more effectively dissipated than the magnetic helicity. This occurs because energy is being transferred to shorter wavelengths where dissipation is more effective, and because an additional energy dissipation process, viscous dissipation, is now available to the magnetofluid. At later times this ratio, E_T/H_M, appears to asymptote toward a lower value than it had initially.

More exact information about the energy dissipation is shown in figure 2, which shows the mean square electric current, the enstrophy, and the fractional heating rate as functions of time. All three of these quantities are seen to rise rapidly at the onset of the turbulent heating process. The electric current density and the vorticity emphasize the high k parts of the magnetic field and velocity field, respectively. Hence the mean square electric current and the enstrophy grow as the magnetofluid becomes turbulent. We will show later that the rapid rise in the mean square electric

current is coincident with the formation of sheets of electric current. In the same way, the rise in the enstrophy is coincident with the generation of concentrated vorticity structures in the vicinity of these electric current sheets. The fractional heating rate, *i.e.*, the logarithmic derivative of the total energy, equals the sum of the enstrophy and mean square electric current divided by the total energy. This rate remains approximately constant until the onset of turbulence, indicating that the dissipation up to this time is not being mediated by nonlinear processes. When the turbulence sets in, a rapid rise in the fractional heating rate occurs, followed by several smaller bursts of activity.

It is of interest that the enstrophy attains such a high value relative to the mean square electric current. Figure 3 shows the ratio of kinetic energy to magnetic energy as a function of time, and the ratio of the enstrophy to the mean square electric current. The initial value of the ratio E_V/E_B is 2.5×10^{-4}, and it attains a maximum value of about 0.1. The ratio of the viscous dissipation to the Ohmic dissipation has an initial value of about 1.0×10^{-3} and attains its maximum value of almost 0.7. Both of these ratios attain their peak values at about the time of greatest heating ($t \approx 30$) as determined by the fractional heating rate of figure 2. Hence, although the kinetic energy is small, the turbulence of the magnetofluid produces a relatively large amount of viscous dissipation. This also implies that a significant amount of heating occurs by a secondary process, *viz.*, the magnetic energy is transformed first into kinetic energy and then into heat energy by viscous dissipation.

Figure 4 exhibits the harmonic history for several of the magnetic energy modes. Initially, most of the magnetic energy is in the (1,1,0) mode (*i.e.*, $(k_x = 1, k_y = 1, k_z = 0)$), for which $\mid \mathbf{k} \mid^2 = 2$. The initial perturbation of the magnetic field is

entirely in modes with $| \mathbf{k} |^2 > 2$, and no energy is in any mode with $| \mathbf{k} |^2 < 2$. The (1,1,0) mode decays Ohmically until the onset of MHD turbulence. After about twenty Alfvén transit times a period of rapid decay of the (1,1,0) magnetic mode occurs. At this time the energy is being transferred out of the (1,1,0) mode to modes with different values of $| \mathbf{k} |^2$ in both the magnetic field and the velocity field by turbulent processes. At the shorter wavelengths the dissipation is more effective. We also see the excitation of certain longer wavelength modes of the system, in particular the (1,0,0) mode and the (0,1,0) mode. For both of these modes $| \mathbf{k} |^2 = 1$. Within the period of a few Alfvén transit times these modes grow so rapidly that their energies each exceed in magnitude the (1,1,0) mode. Excitation of the (0,0,1) mode is comparatively negligible. The morphological consequence of this turbulent transfer of energy is shown in figure 5, which shows contours of constant z magnetic field at times early and late in the numerical simulation. This excitation of the lower $| \mathbf{k} |^2$ modes is similar to that derived by Browning *et al.* (1986).

The processes which contribute to the accelerated heating are illuminated by examination of two-dimensional slices taken through the system perpendicular to the z direction at $(x, y, z = 0)$. For several important times we show plots of B_x and B_y, J_z, u and v, and ω_z. Figure 6 shows these fields at $t = 0.5$, a time prior to the onset of the rapid heating. The state of the fields at this time is very similar to the initial conditions. The magnetic field (B_x, B_y) and electric current density (J_z) are similar in appearance due to the almost force-free character of the magnetic field. However, the electric current density (J_z) appears more perturbed because it emphasizes the high wavelength components of the magnetic field. These fields are close to zero in the centre of the plot and at the corners. No electric current sheets are present initially. The velocity field (u, v) and vorticity (ω_z) are relatively

random in appearance. This also reflects their initial conditions. Note the absence of long-wavelength structure in the velocity field (u, v) and vorticity field (ω_z), and the lack of correlation with the magnetic field (B_x, B_y).

Figure 7 shows these fields at $t = 25$, during the phase of rapid heating. Two changes in the magnetic field (B_x, B_y) configuration are apparent, *viz.*, the shifting of the field so that regions of oppositely directed field are adjacent, and emergence of larger scales in the magnetic field. One merger is occuring at the center of the plots, the other is occuring at the corners. Since these mergers are similar we will restrict discussion to the one occuring in the centre of the plot. Note that since the magnetic field is not confined by walls it is free to reconfigure itself in this fashion. The merging of the magnetic field is mediated by the large electric current sheet which forms between the merging regions. This sheet carries electric current of sign opposite to the electric current in the merging regions. The maximum amplitude of the electric current density (J_z) in the sheet is four to five times that of the initial maxima. It is the formation of these sheets that leads to the increase in the mean square electric current at this time (figure 2). Large scale, organized fluid motions also are now seen in (u, v). These fluid motions serve to drag magnetic flux into the electric current sheet, increasing the reconnection rate and hence the heating rate. Note also the flows out of the reconnection zone, with speeds a significant fraction of the Alfvén speed. A quadrupolar vorticity distribution in (ω_z) is seen to form in the vicinity of the electric current sheet. The vorticity (ω_z) maxima at this time are over thirty times greater than their initial value. The viscous dissipation of energy is very strong in these regions of large vorticity, and this is evidenced by the increase in enstrophy seen after about $t = 20$ (figure 2).

Figure 8 shows these fields at the final time in the simulation, $t = 53$. At this time most of the turbulent activity has ceased. The magnetic field (B_x, B_y) is now dominated by the largest scales in the system. This also can be inferred from a comparison of figure 1 and figure 4. At this time the electric current density (J_z) has decreased in value, the maxima being about one third of their original value. Although the electric current density is noisy, its form appears to be similar to that of the magnetic field – a characteristic to be expected in a force-free state. The electric current sheets which produced the accelerated dissipation have disappeared. The velocity field (u, v) still possesses some long wavelength structure, but its magnitude has declined. The vorticity field (ω_z) now has an appearance similar to the electric current density with no concentrated vorticity structures evident, and the maxima of both J_z and ω_z are of similar magnitude.

One feature of interest is the behavior of α in the force-free regions. We show slice plots of α and the force-free regions in the $(x, y, z = 0)$ plane which indicate that α varies significantly in the force-free regions. Figure 9 shows α and the force free regions at $t = 0.5$ and $t = 53$. To delineate the force free regions, we plot $(\mathbf{J} \cdot \mathbf{B})/(\mid \mathbf{J} \mid^2 \mid \mathbf{B} \mid^2)^{\frac{1}{2}}$. This quantity will have a magnitude of 1 in the force-free regions. To show the spatial distribution of α, we plot $(\mathbf{J} \cdot \mathbf{B})/(\mathbf{B} \cdot \mathbf{B})$. Recall that $\alpha = 2^{\frac{1}{2}}$ for the magnetic field given by equations $6a - 6c$. At $t = 0.5$ the magnetic field is almost entirely force free except for small regions near the centre and at the corners of the plot. These are the regions in which $\mathbf{B}$ is close to zero. At the same time, some variation in α is seen throughout the force-free regions. The variation in α is due to the initial perturbation, and, as might be expected, the largest variation is seen in the regions which are not force-free. At $t = 53$, the magnetic field has

evolved to a new state which has large regions that are force-free. Substantially more variation in α is evident, especially near the corners of the plot.

We have performed these simulations at $S = M = 50, 100$, and 200 with essentially the same results. In the absence of nonlinear effects, raising S slows down the decay of the background magnetic field. In the presence of nonlinear effects, raising the Lundquist numbers, M and S increases the strength of the nonlinear terms relative to the dissipative terms. This allows the magnetofluid to transfer excitations to short wavelengths more efficiently. Hence, as the Lundquist numbers are raised, the peak magnitudes of the electric current sheet and the concentrated vorticity structures tend to increase. This leads to larger peak values of the mean square electric current and enstrophy, with a corresponding larger loss of magnetic energy during the phase of rapid dissipation. The heating contribution due to enstrophy generation is significant in all of these runs. Variation in α also was seen throughout all of the runs performed. We also have used other sets of random perturbations, and again obtained essentially the same results. A full parameter search is impractical because of the expense of these calculations.

5. Discussion

In this paper we report the results of numerical simulations of the decay of turbulence in a magnetofluid with a high degree of magnetic helicity present initially. Similar magnetofluid configurations are believed to be present in the solar corona, and perhaps to underlie the process by which the solar corona is heated (*cf.* Heyvaerts and Priest 1984). Our motivation for performing these numerical simulations was to understand better the dynamical evolution and energetics of a helically turbulent magnetofluid, and to identify the structures which develop during the course of this evolution. For the foreseeable future, numerical simulations appear to be the best way of obtaining such insight, since direct measurement of the magnetic field and velocity field in the solar corona is not possible at present. The ideal invariants (equations $2a-2c$) have been measured in the solar wind by means of *in situ*, single point covariances (*e.g.*, Matthaeus and Goldstein 1982). However, the most common methods for determining the coronal magnetic field and velocity field are indirect. The coronal magnetic field is commonly extrapolated from the longitudinal component of the photospheric field, under the assumption that it is either a potential magnetic field or a force-free magnetic field. The coronal velocity field generally is extrapolated from Doppler-shift measurements of the line-of-sight velocity field component in the transition region. Simultaneous specification of both of these fields at the same point in the corona is at present out of the question. Analysis of helically turbulent magnetofluids is also difficult, primarily due to the complexity of the governing nonlinear, partial differential equations. Even very simple, deterministic, initial conditions can lead to analytically intractable behavior after a few Alfvén transit times (*e.g.*, Pouquet *et al.* 1986). A promising start

in the analytic direction has been made by Krishan (1985), who has formulated a statistical mechanics for active region coronal magnetofluids. In light of the state of observations and analysis, we have chosen not to concentrate our efforts on the investigation of an elaborate model. Instead, we have investigated a relatively simple magnetohydrodynamic configuration which possesses the most significant feature, *viz.*, twisted magnetic fields, and have attempted to understand the important features of its evolution. This approach concedes two present-day limitations of direct numerical simulations of turbulent fluids: the restriction to simple geometries and the restriction to low Lundquist (or Reynolds) numbers.

Our numerical simulations have shown that accelerated dissipation of magnetic energy occurs in a magnetofluid with a high degree of magnetic helicity present initially and with open boundary conditions. Large regions remain force-free during the entire evolution of the magnetofluid. The initial magnetic configuration has no electric current sheets present, but it evolves toward a state in which electric current sheets do exist. In this respect, the boundary conditions seem to be important because they allow the "tubes" to slide around each other. Formation of the electric current sheet produces non-negligible Lorentz forces. High speed flows develop which sweep additional magnetic flux into the region of the electric current sheet, leading to an accelerated dissipation of magnetic energy. It is in the vicinity of the non-force-free field regions that the bulk of the accelerated heating occurs. The final form of the magnetic field appears to be dominated by the largest length scales allowed in the system (compare figure 1 and figure 4). The structural evolution of the magnetic field and the electric current density, combined with the selective decay of the total energy with respect to the magnetic helicity (figure 1), suggest that the magnetofluid is self-organizing in the manner described in Sect. 2.

We also note that the magnetofluid velocity plays a significant role in the evolution of the system. When the Lorentz force becomes non-negligible, high speed flows develop. The highest level of kinetic energy is achieved during the time of the formation of the electric current sheets, at which time the kinetic energy is about 10 % of the magnetic energy. The high level of kinetic energy does not seem to inhibit the self-organization of the magnetofluid, *e.g.*, the total energy decays selectively with respect to the magnetic helicity in a monotonic fashion (figure 1). However, the numerical simulations imply that the magnetofluid cannot be modelled as evolving quasi-statically (*e.g.*, Heyvaerts and Priest 1984), and that fluid motions must be taken into account.

Accompanying the increase in kinetic energy is an increase in enstrophy, which peaks at about 70 % of the mean square electric current during the time of greatest heating. Hence, viscous heating also contributes significantly to the accelerated dissipation rate (*cf.* Rosner *et al.* 1986). We have performed our numerical simulation with unit magnetic Prandtl number. However, in the solar corona the magnitude of the kinematic viscosity is estimated to exceed the magnetic diffusivity (*e.g.*, Pneuman and Orrall 1986). This implies that the heating due to viscous dissipation might be greater than that due to Ohmic dissipation. The rise in enstrophy is directly related to the formation of concentrated structures in the vorticity, which in this case take the form of a "quadrupolar prism" (similar in form to structures found in two dimensions, *cf.* Matthaeus 1982). These structures are similar to the electric current sheets with respect to dissipation, *viz.*, within them the vorticity can become so large that even at very low viscosities it is possible to dissipate large amounts of kinetic energy. Our simulations appear to show that these concentrated

vorticity structures are as important in the coronal heating process as are electric current sheets.

Another feature of interest is the temporal behavior of α, the ratio of the electric current density to the magnetic field. Our numerical results indicate that α does not approach a constant value after the time of rapid heating, as suggested by the theory of Heyvaerts and Priest (1984). Rather, although the magnetofluid quickly returns to a state that can be characterized as mostly force-free, it is not observed to return to a state for which the electric current density and the magnetic field are topologically identical. Thus, the accelerated heating occurs as the system evolves through a series of force-free states, but not through a series of constant α states. We suggest that an explanation for this may lie in the direct action of fluid motions. When the Lorentz force in the magnetofluid becomes locally non-negligible, fluid motions are excited. Generally, the evolving velocity field will not be aligned with the magnetic field, and hence it will perturb the magnetic field away from any constant α force-free state through the perturbed electric field term, $\mathbf{v} \times \mathbf{B}$, in the magnetic equations. When the Lorentz force term becomes weaker as a consequence of the fluid motions and dissipative losses, the fluid acceleration also decreases until the $\mathbf{J} \times \mathbf{B}$ force term has entirely disappeared and the fluid is again nearly at rest. The resulting nearly quiescent state must be force-free but not necessarily constant α, which fits the final states from our simulations. This implies that a constant α approximation must be applied with great caution.

We are currently extending this work to two additional cases of interest to the solar physics community. First, we wish to determine the influence of a constant magnetic field on the results reported here. Second, we are determining the evolution of this system when it is subjected to constant injection of magnetic helicity.

both with and without the presence of a non-self-consistent magnetic field component. This situation is analogous to the twisting of the coronal footpoints by fluid motions in the photosphere (*e.g.,* Parker 1982, Browning *et al.* 1986). Finally, the addition of compressible effects and radiation to the model is of interest (Pettini *et al.* 1985; R. Dahlburg *et al.* 1986*b*, 1987, Karpen *et al.* 1987).

Acknowledgements. The authors gratefully acknowledge helpful discussions with Dr. T. A. Zang, Dr. J. M. Picone, Dr. D. C. Montgomery, Dr. J. A. Klimchuk, Dr. J. T. Karpen, Dr. J. H. Gardner, Dr. J. P. Boris, and Dr. S. K. Antiochos. This work was sponsored in part by the National Aeronautics and Space Administration Solar Terrestrial Theory Program and by the Office of Naval Research. J. P. D. acknowledges support under National Aeronautics and Space Administration Grant NAG-W-710 while on leave at Dartmouth College. The numerical simulations were performed on the NASA Ames Research Center CRAY-2. Supporting numerical simulations were performed on the NRL CRAY-XMP/24 by means of a grant of computer time from the Director of Research of the Naval Research Laboratory.

Appendix

Numerical algorithm

Since we are considering a fully periodic magnetofluid, it is appropriate to use a Fourier pseudospectral method for the spatial discretization (Gottleib and Orszag 1977). In the customary fashion, we evaluate all spatial derivatives, without phase error, in the relevant partial Fourier space. The nonlinear product terms are evaluated most easily in configuration space. We use the vectorized fast Fourier transform algorithm of Temperton (1983) to move between configuration space and Fourier space. We note that pseudospectral methods have been applied with great success to a variety of hydrodynamic and magnetohydrodynamic turbulence and transition problems (see the recent review by Zang and Hussaini 1987).

The equations with time derivatives, 1*a* and 1*c*, are written in the rotation form. In the ideal case, the discretized form of these equations is said to semi-conserve energy – in the sense that the only errors in the energy conservation are due to the time discretization. A consequence of this energy conservation property is improved stability of the numerical method. A formal proof of this point is given by T. A. Zang in an appendix of J. Dahlburg *et al.* (1986*a*) (see also Gottleib and Orszag 1977).

For our calculation we find it convenient to enforce the solenoidality of the velocity and magnetic vector potential fields indirectly by means of the appropriate Poisson equations (Note that the solenoidality of the magnetic induction field is enforced trivially, *i.e.*, $\nabla \cdot \mathbf{B} = \nabla \cdot \nabla \times \mathbf{A} = 0$). Taking the divergence of equations 1*a* and 1*c* gives the result:

$$\nabla^2 \Pi = \nabla \cdot \mathbf{H}, \tag{A1a}$$

$$\nabla^2 \Phi = -\nabla \cdot \mathbf{G}. \tag{A1b}$$

Solving the Poisson equations $A1a$ and $A1b$ for Π and Φ ensures the solenoidality of the velocity and magnetic vector potential fields (see R. Dahlburg *et al.* 1986*a*).

In order to explicate more fully the numerical method, we first rewrite equations 1*a* and 1*c*:

$$\frac{\partial \mathbf{v}}{\partial t} = \mathbf{H}, \tag{A2a}$$

$$\frac{\partial \mathbf{A}}{\partial t} = \mathbf{G}. \tag{A2b}$$

We time advance **v** and **A** by a second order Runge Kutta scheme. For example, consider the x component of the velocity field, $u(\mathbf{x}, t)$. For $\frac{du}{dt} = H_x(\mathbf{v}, \mathbf{A}, t)$, the time discretization gives:

$$u^{n+\frac{1}{2}} = u^n + \frac{\Delta t}{2} H_x^n(\mathbf{v}^n, \mathbf{A}^n, t^n), \tag{A3a}$$

$$u^{n+1} = u^{n+\frac{1}{2}} + (\Delta t) H_x^{n+\frac{1}{2}}(\mathbf{v}^{n+\frac{1}{2}}, \mathbf{A}^{n+\frac{1}{2}}, t^{n+\frac{1}{2}}), \qquad (A3b)$$

where the superscript n indexes the time level. In the absence of dissipation, the temporal discretization is known to be weakly unstable, but this should not affect integration to the time levels that we consider here. A full discussion of the stability and accuracy properties of this time-stepping scheme is given by J. Dahlburg *et al.* (1985).

The Poisson equations, $A1a$ and $A1b$, are easily inverted in the full Fourier space, where they become:

$$k^2 \Pi(\mathbf{k}, t) = -i\mathbf{k} \cdot \mathbf{H}(\mathbf{k}, t), \qquad (A4a)$$

$$k^2 \Phi(\mathbf{k}, t) = i\mathbf{k} \cdot \mathbf{G}(\mathbf{k}, t). \qquad (A4b)$$

In summary, we first solve for Π and Φ at the previous time level n. We then time-advance $\mathbf{v}$ and $\mathbf{A}$ to the time level $n + \frac{1}{2}$. Then we solve for Π and Φ at the time level $n + \frac{1}{2}$. Using these values for the time level $n + \frac{1}{2}$ we perform the full time-step on $\mathbf{v}$ and $\mathbf{A}$ to the time level $n + 1$.

References

Bondeson, A., and Sobel, J. R.: 1984, *Phys. Fluids* **27**, 2028

Browning, P. K., Sakurai, T., Priest, E. R.: 1986, *Astron. Astrophys.* **158**, 217

Browning, P. K., Priest, E. R.: 1986, *Astron. Astrophys.* **159**, 129

Dahlburg, J. P., Montgomery, D., Matthaeus, W. H.: 1985, *J. Plasma Phys.* **34**, 1

Dahlburg, J. P., Montgomery, D., Doolen, G. D., Matthaeus, W. H.: 1986*a*, *J. Plasma Phys.* **35**, 1

Dahlburg, J. P., Montgomery, D., Doolen, G. D., Turner, L.: 1986*b*, *Phys. Rev. Lett.* **57**, 428

Dahlburg, J. P., Montgomery, D., Doolen, G. D., Turner, L. 1987, *J. Plasma Phys.* **37**, 299

Dahlburg, R. B., Zang, T. A., Montgomery, D., Hussaini, M. Y.: 1983, *Proc. Nat. Acad. Sci. USA* **80**, 5798

Dahlburg, R. B., Zang, T. A., Montgomery, D.: 1986*a*, *J. Fluid Mech.* **169**, 71

Dahlburg, R. B., Picone, J. M., Mariska, J. T.: 1986*b*, *NRL Memo. Rep.* **5911**

Dahlburg, R. B., DeVore, C. R., Picone, J. M., Mariska, J. T., Karpen, J. T.: 1987, *Astrophys. J.* **315**, 385

Forbes, T. G., Priest, E. R.: 1983, *Solar Phys.* **84**, 169

Frisch, U., Pouquet, A., Leorat, J., Mazure, A.: 1975, *J. Fluid Mech.* **68**, 769

Gottleib, D., Orszag, S. A.: 1977, *Numerical Analysis of Spectral Methods: Theory and Applications, NSF-CBMS mon.* no. 26. Soc. Ind. App. Math., Philadelphia

Hasegawa, A.: 1985, *Adv. Phys.* **34**, 1

Heyvaerts, J., Priest, E. R.: 1984, *Astron. Astrophys.* **137**, 63

Horiuchi, R., Sato, T.: 1985, *Phys. Rev. Lett.* **55**, 211

Horiuchi, R., Sato, T.: 1986, *Phys. Fluids* **29**, 1161

Karpen, J. T, Picone, J. M., Dahlburg, R. B.: 1987, *Astrophys. J.* in press

Krishan, V.: 1985, *Solar Phys.* **95**, 269

Low, B. C.: 1982, *Revs. Geophys. Space Phys.* **20**, 145

Matthaeus, W. H., Montgomery, D.: 1980, *Ann. Rev. N.Y. Acad. Sci.* **357**, 203

Matthaeus, W. H., Montgomery, D.: 1981, *J. Plasma Phys.* **25**, 11

Matthaeus, W. H., Goldstein, M. L.: 1982, *J. Geophys. Res.* **87**, 6011

Matthaeus, W. H.: 1982, *Geophys. Res. Lett.* **9**, 660

Meneguzzi, M., Frisch, U., Pouquet, A.: 1981, *Phys. Rev. Lett.* **47**, 1060

Montgomery, D., Turner, L., Vahala, G.. 1978, *Phys. Fluids* **21**, 757

Parker, E. N.: 1982, *Geophys. Astrophys. Fluid Dynamics* **22**, 195

Pettini, M., Nocera, L., Vulpiani, A.: 1985, in *Chaos in Astrophysics*, ed. J. R. Buchler, J. M. Perdang, and E. A. Spiegel, Reidel, Dordrecht

Pouquet, A., Frisch, U., Leorat, J.: 1976, *J. Fluid Mech.* **77**, 321

Pneuman, G. W., Orrall, F. Q.: 1986, in *Physics of the Sun*, ed. P. A. Sturrock, T. E. Holzer, D. M. Mihalas, and R. K. Ulrich, Reidel, Dordrecht

Priest, E. R.: 1982, *Solar Magnetohydrodynamics*, Reidel, Dordrecht

Rosner, R., Low, B. C., and Holzer, T. E.: 1986, in *Physics of the Sun*, ed. P. A. Sturrock, T. E. Holzer, D. M. Mihalas, and R. K. Ulrich, Reidel, Dordrecht

Spicer, D. S., Mariska, J. T., and Boris, J. P.: 1986, in *Physics of the Sun*, ed. P. A. Sturrock, T. E. Holzer, D. M. Mihalas, and R. K. Ulrich, Reidel, Dordrecht

Syrovatskii, S. I.: 1978, *Solar Phys.* **58**, 89

Taylor, J. B.: 1974, *Phys. Rev. Lett.* **33**, 1139S

Taylor, J. B.: 1986, *Revs. Mod. Phys.* **58**, 741

Temperton, C.: 1983, *J. Comp. Phys.* **52**, 1

Zang, T. A., Hussaini, M. Y.: 1987, *Ann. Rev. Fluid. Mech.* 19 339

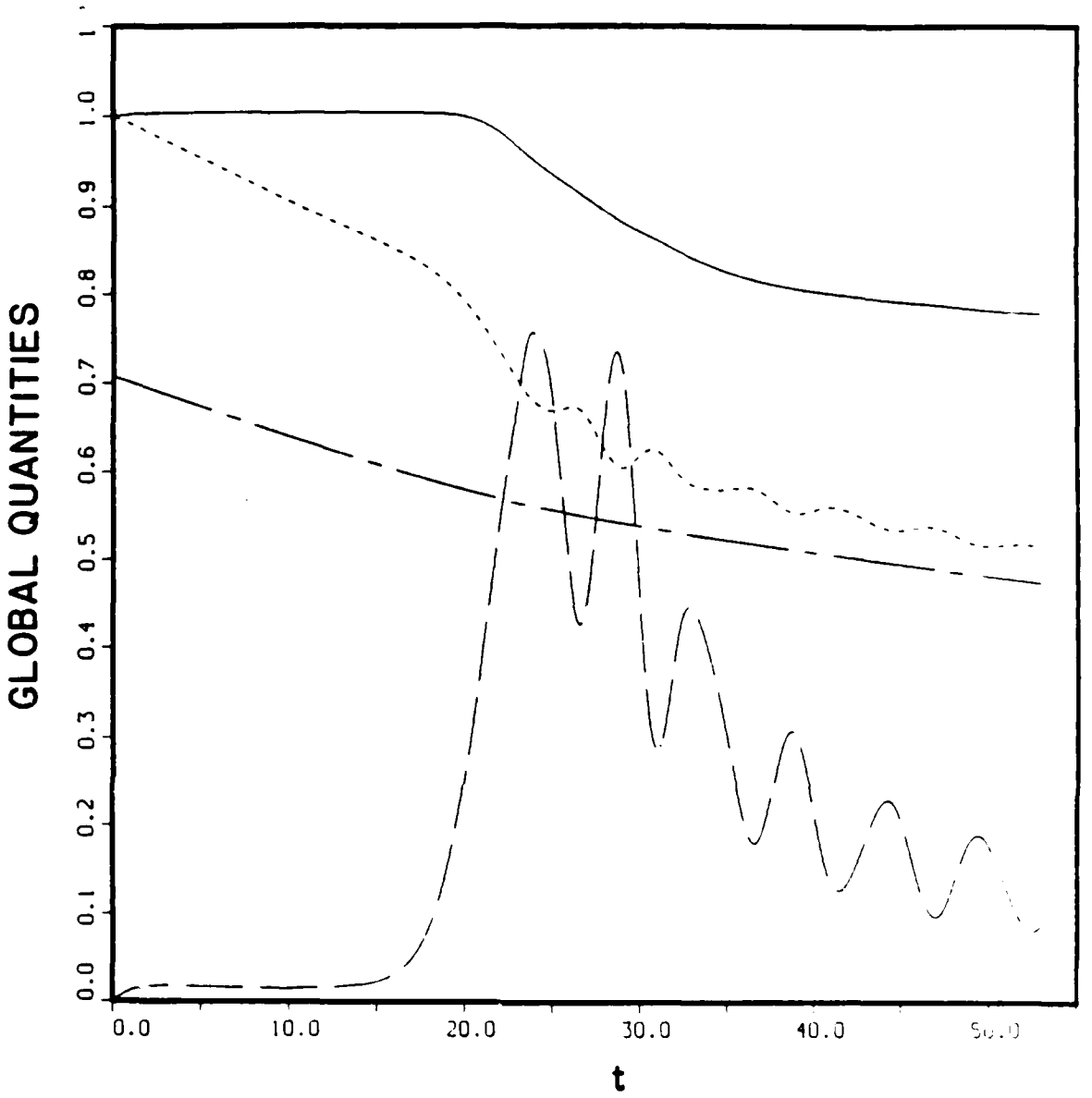

Figure 1. Plot of global quantities *vs* time. Dashed line: magnetic energy; Dash-dot line: kinetic energy times ten; Mixed dash line: magnetic helicity. Solid line: ratio of total energy to magnetic helicity.

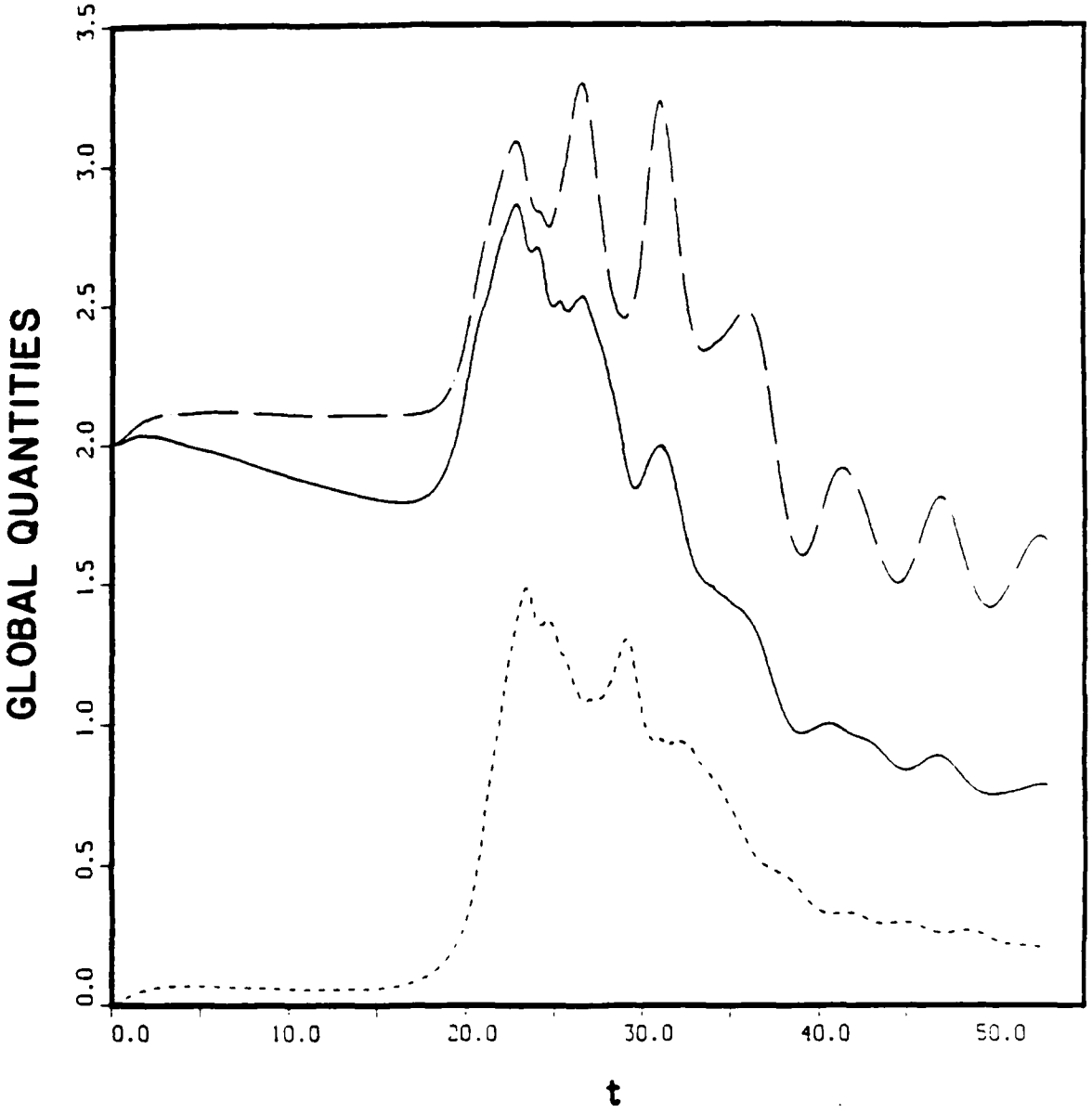

Figure 2. Plot of global quantities *vs* time. Solid line: mean square electric current; Dashed line: enstrophy; Dash-dot line: fractional heating rate.

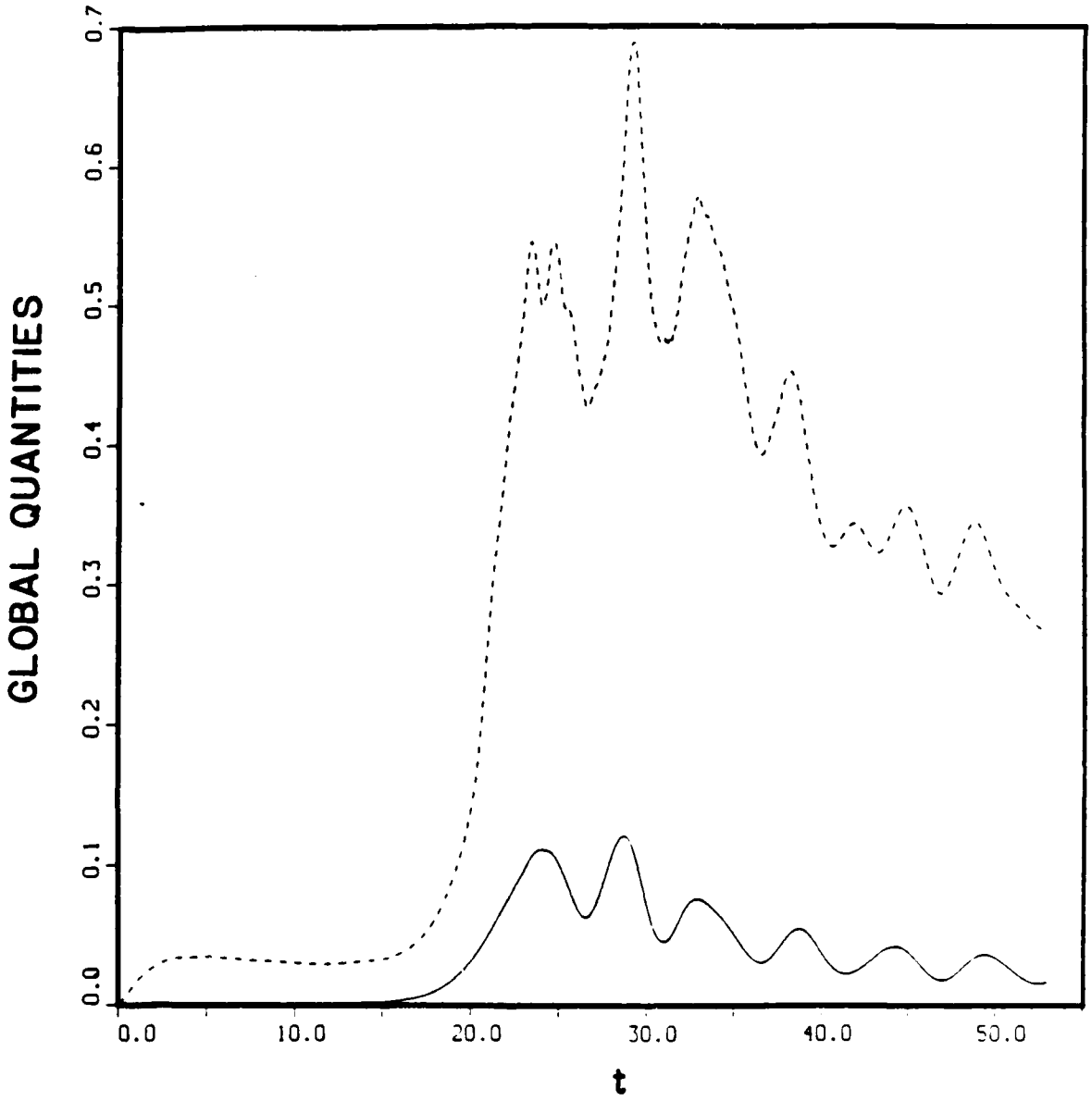

Figure 3. Plot of global quantities *vs* time. Solid line; Ratio of kinetic energy to magnetic energy; Dashed line: Ratio of enstrophy to mean square electric current.

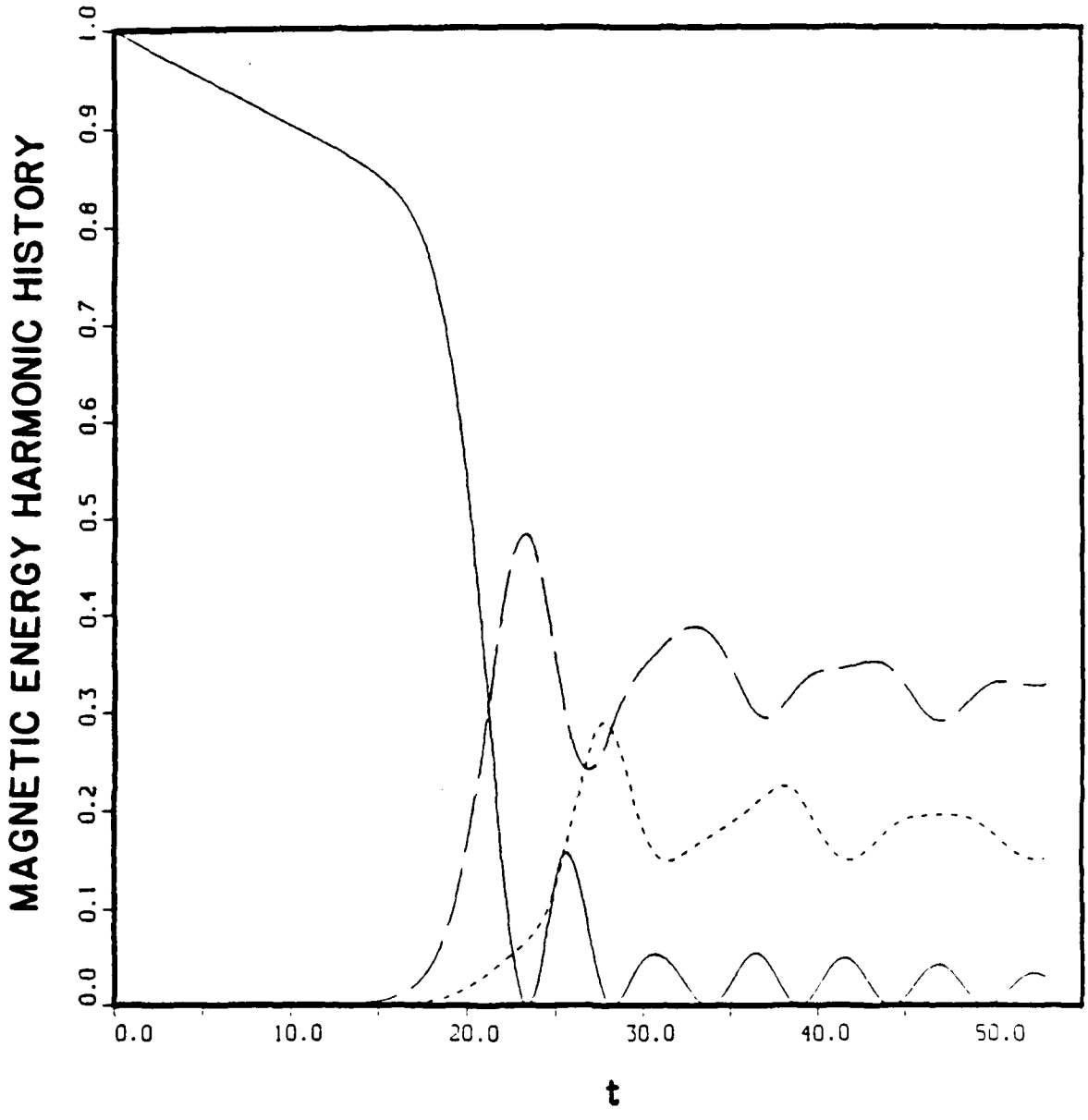

Figure 4. Plot of magnetic energy harmonic histories. Solid line: (1,1,0) mode; Dashed line: (1,0,0) mode; Dash-dot line: (0,1,0) mode.

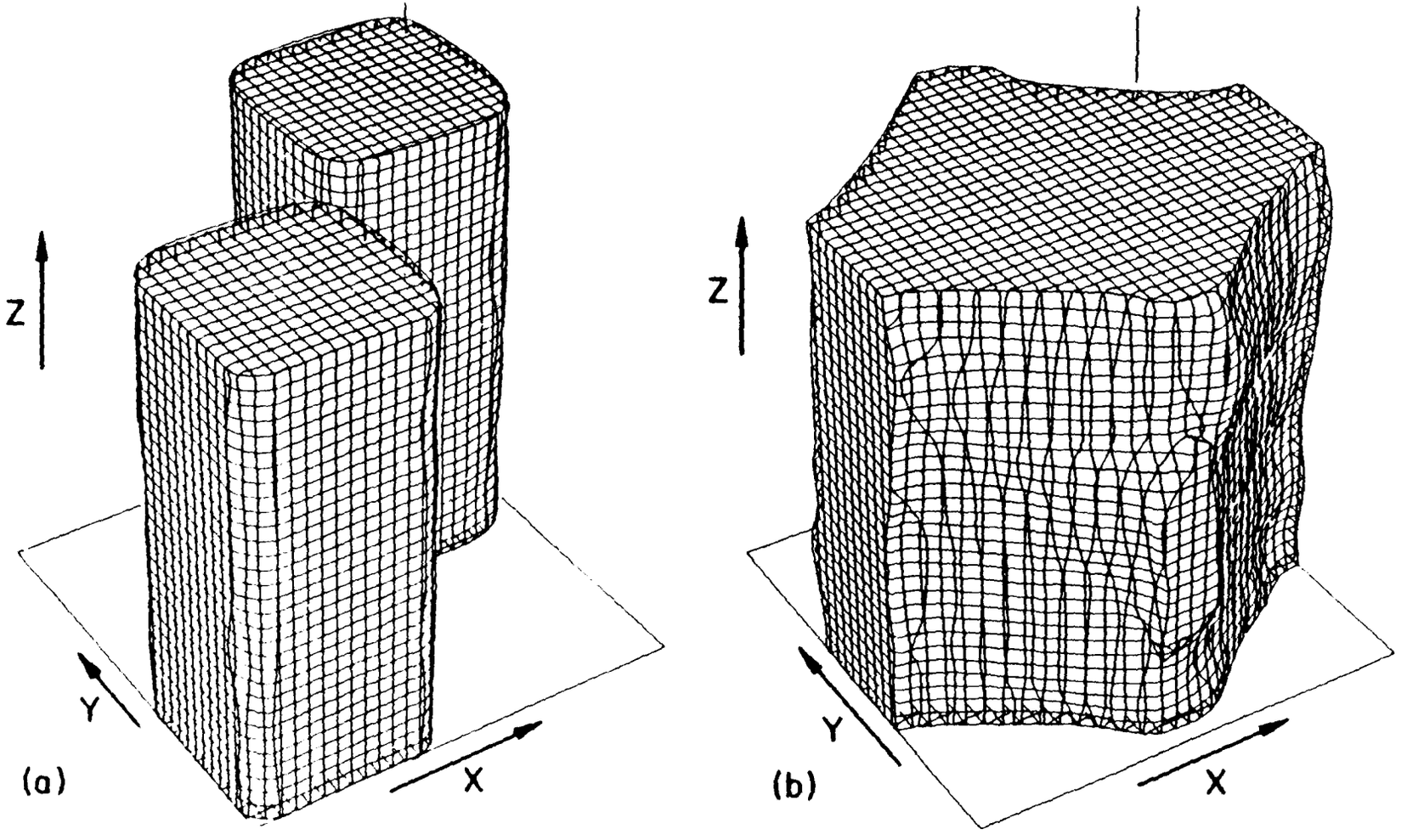

Figure 5. Plots of constant z magnetic field; *a.* $t = 0.5$; *b.* $t = 53$.

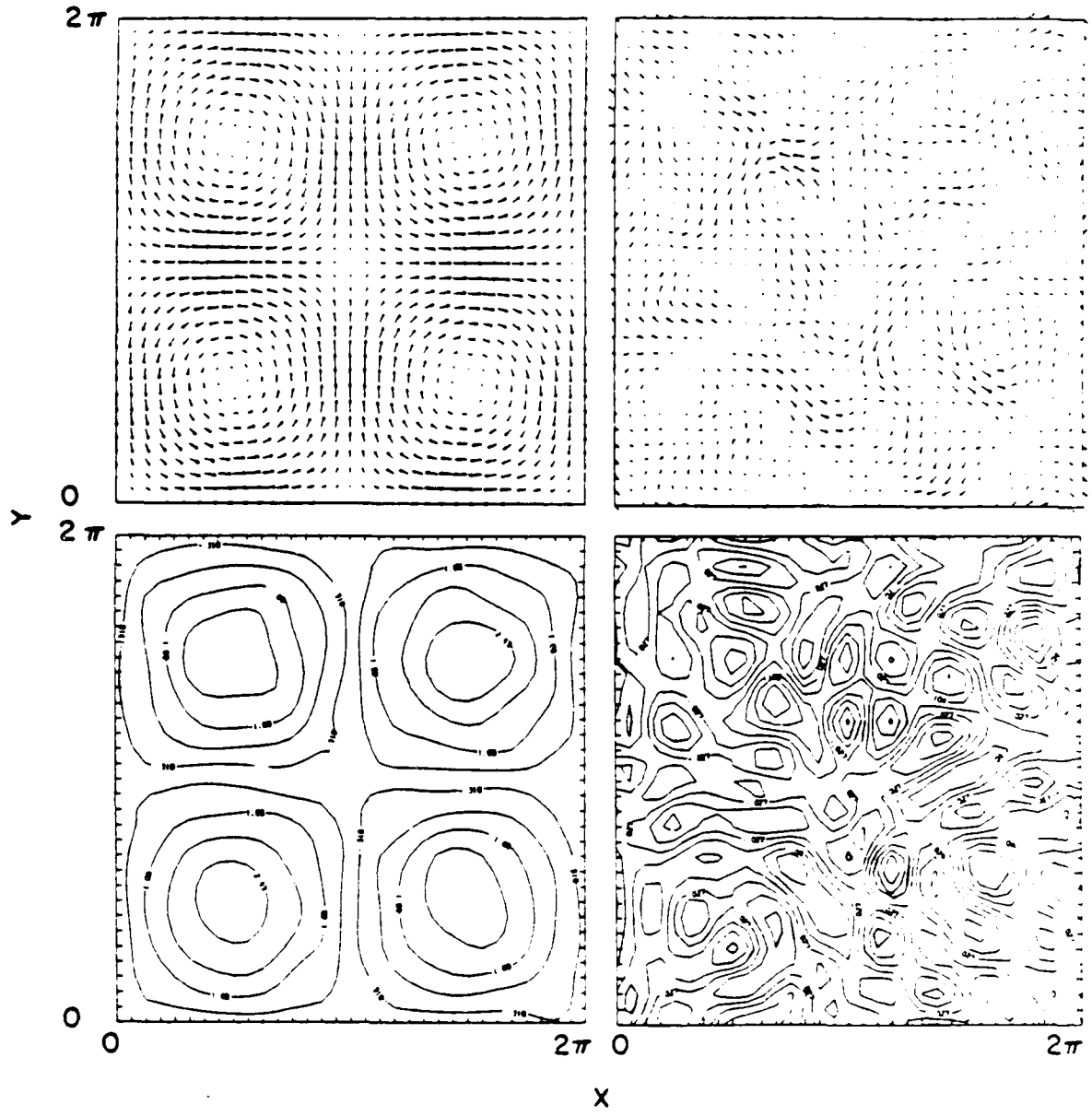

Figure 6. Plots in $(x, y, z = 0)$ plane at $t = 0.5$. *top left*. Vector plot of B_x and B_y, maximum magnetic field = 1.44. *top right*. Vector plot of u and v, maximum velocity = 0.138. *bottom left*. Contour plot of j_z, maximum contour = 2.43, minimum contour = -2.38. *bottom right*. Contour plot of ω_z, maximum contour = 0.235, minimum contour = -0.223.

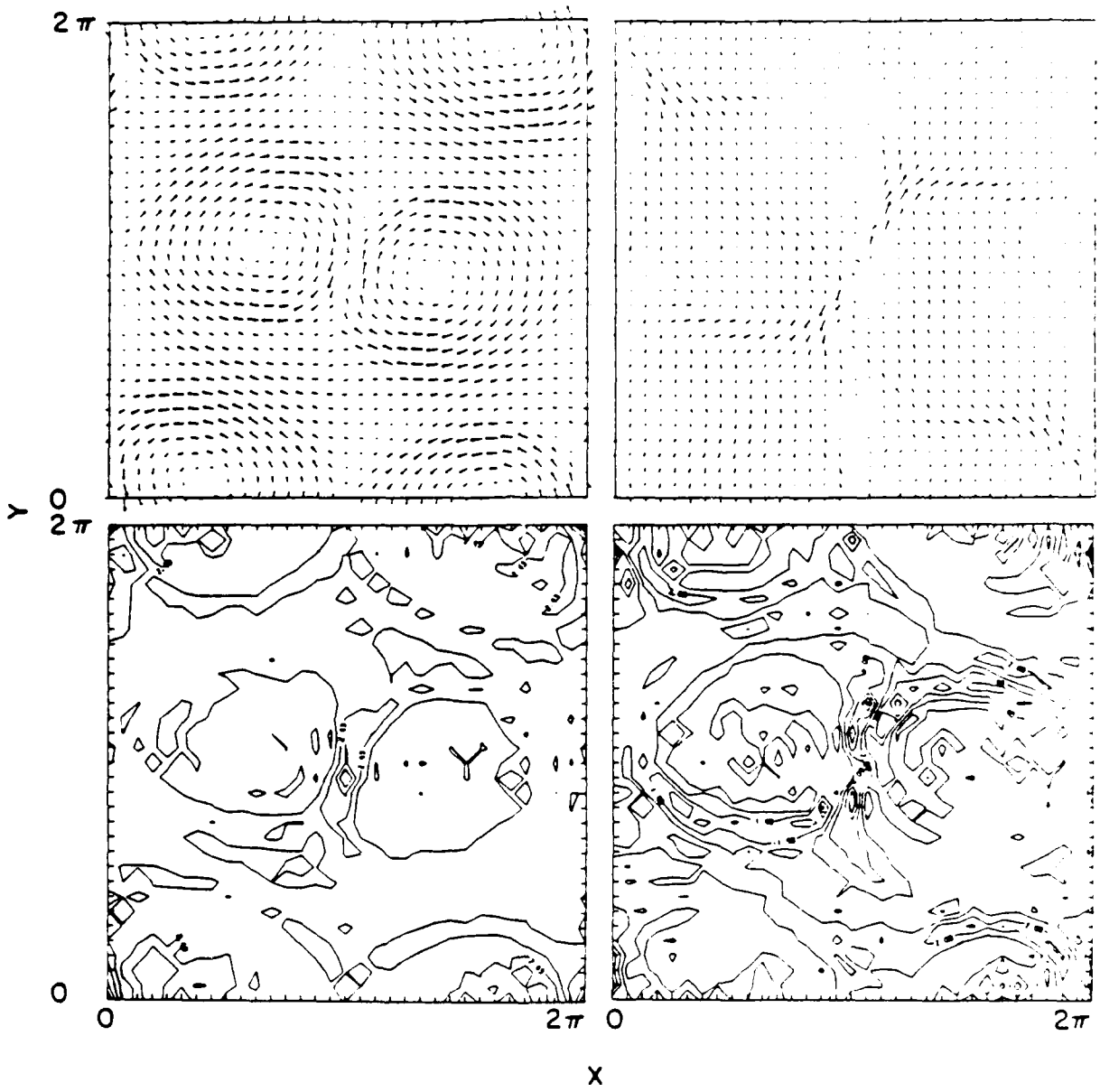

Figure 7. Same as figure 6 at $t = 25$. *top left*. Maximum magnetic field = 1.50. *top right*. Maximum velocity = 1.25. *bottom left*. Maximum contour = 0.25, minimum contour = -14.6 *bottom right*. Maximum contour = 7.32, minimum contour = -6.63.

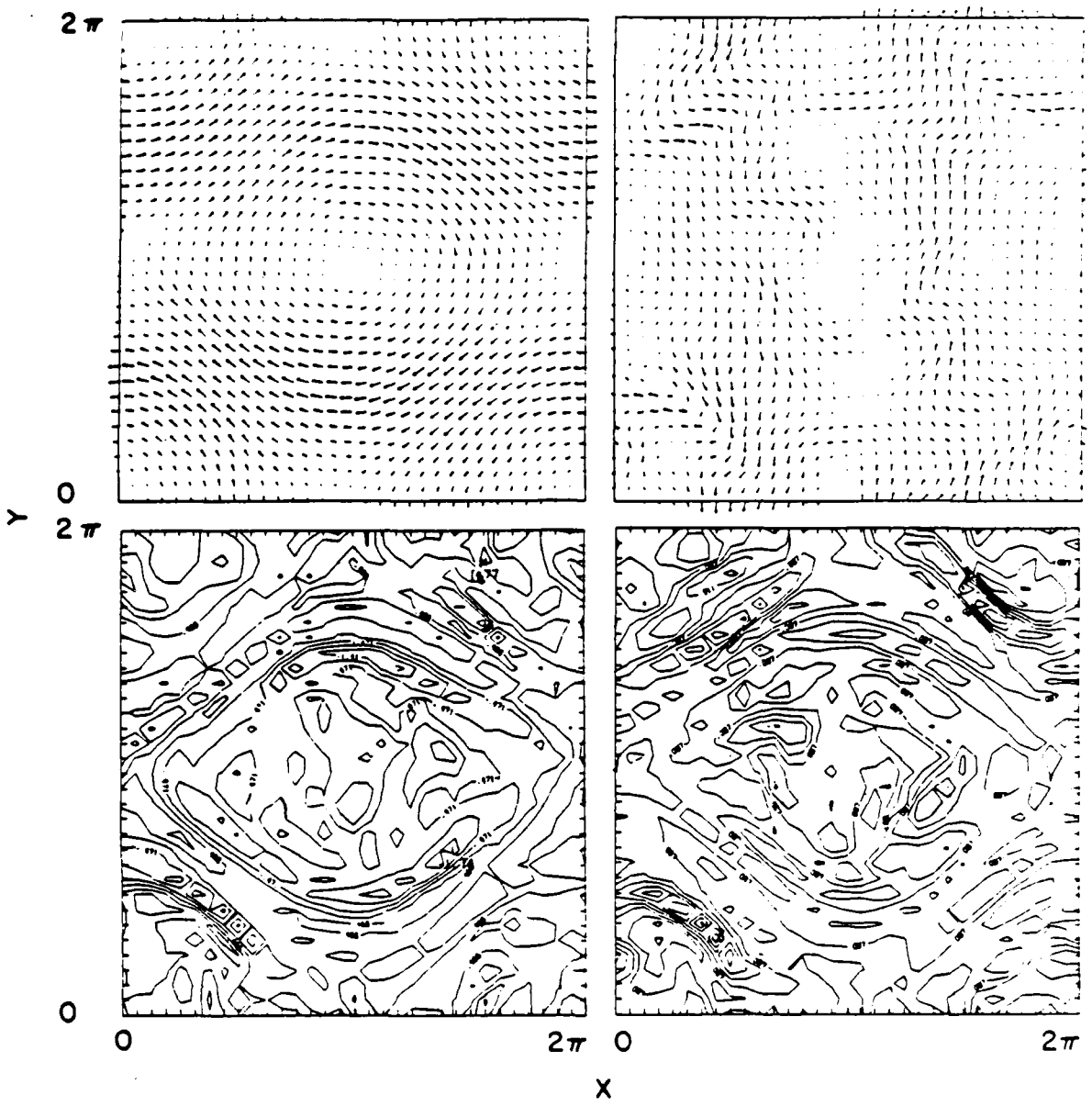

Figure 8. Same as figure 6 at $t = 53$. *top left*. Maximum magnetic field = 1.03. *top right*. Maximum velocity = 0.36. *bottom left*. Maximum contour = 1.87, minimum contour = -1.87 *bottom right*. Maximum contour = 1.92, minimum contour = -1.97.

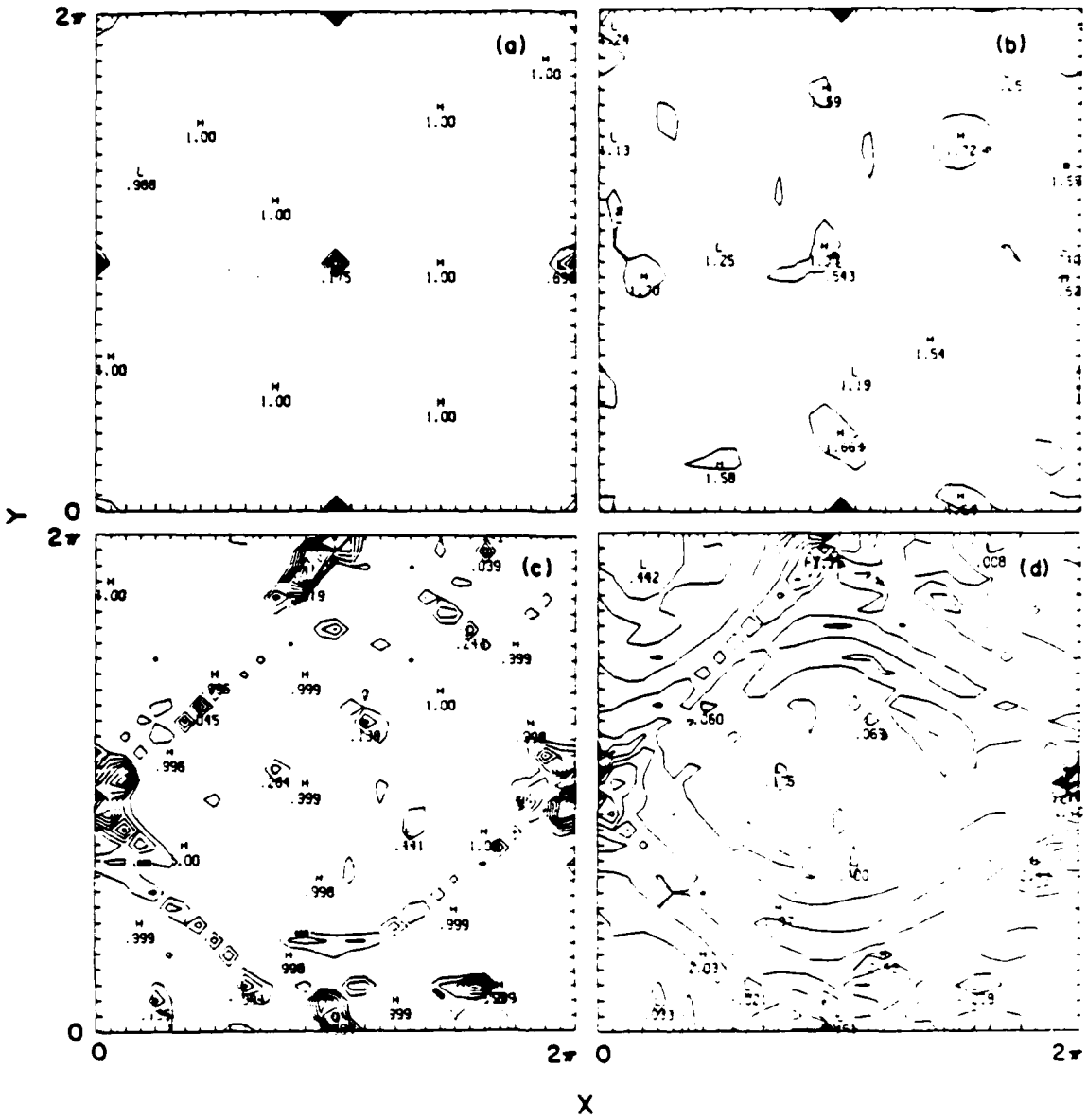

Figure 9. Contour plots in $(x, y, z = 0)$ plane. *a*. Alignment cosine at $t = 0.5$, maximum contour = 0.910, minimum contour = -0.528. A magnitude of 1 indicates that the magnetic field is aligned with the electric current density. *b*. α at $t = 0.5$. maximum contour = 2.51, minimum contour = -5.19. *c*. Alignment cosine at $t = 53$. maximum contour = 0.668, minimum contour = -0.879. *d*. α at $t = 53$. maximum contour = 4.62, minimum contour = -2.28.

END

FILMED

FEB. 1988

DTIC